

Modeling diffusion limitation of gas exchange in lungs containing perfluorocarbon

ELISABETH MATES VANLÖBENSELS,¹ JOSEPH C. ANDERSON,² JACOB HILDEBRANDT,¹
AND MICHAEL P. HLASTALA¹

Departments of ¹Physiology and Biophysics and ²Chemical Engineering, University of Washington,
Seattle, Washington 98195

VanLöbensels, Elisabeth Mates, Joseph C. Anderson, Jacob Hildebrandt, and Michael P. Hlastala. Modeling diffusion limitation of gas exchange in lungs containing perfluorocarbon. *J. Appl. Physiol.* 86(1): 273–284, 1999.—We reported changes in alveolar-arterial P_{O_2} gradient, ventilation-perfusion heterogeneity, and arterial-alveolar PCO_2 gradient during partial liquid ventilation (PLV) in healthy piglets (E. A. Mates, P. Tarczy-Hornoch, J. Hildebrandt, J. C. Jackson, and M. P. Hlastala. In: *Oxygen Transport to Tissue XVII*, edited by C. Ince. New York: Plenum, 1996, vol. 388, p. 585–597). Here we develop two mathematical models to predict transient and steady-state (SS) gas exchange conditions during PLV and to estimate the contribution of diffusion limitation to SS arterial-alveolar differences. In the simplest model, perfluorocarbon is represented as a uniform flat stirred layer and, in a more complex model, as an unstirred spherical layer in a ventilated terminal alveolar sac. Time-dependent solutions of both models show that SS is established for various inert and respiratory gases within 5–150 s. In fluid-filled unventilated terminal units, all times to SS increased sometimes by hours, e.g., SF_6 exceeded 4 h. SS solutions for the ventilated spherical model predicted minor end-capillary disequilibrium of inert gases and significant disequilibrium of respiratory gases, which could explain a large portion of the arterial-alveolar PCO_2 gradient measured during PLV (14). We conclude that, during PLV, diffusion gradients for gases are generally small, except for CO_2 .

liquid breathing; perfluorocarbon liquids; mathematical model; gas exchange

PARTIAL LIQUID VENTILATION (PLV) is a technique of ventilatory support in which the air spaces of the lung are partially replaced with liquid perfluorocarbon (PFC) and then periodically insufflated with O_2 -enriched gas with use of a conventional mechanical ventilator. PLV was first described by Fuhrman et al. (3) and has been shown to improve oxygenation and lung mechanics in animal models and in humans with acute respiratory distress syndrome (2, 4, 8, 10, 11). We previously showed that PLV in healthy piglets causes mild increases in arterial-alveolar P_{O_2} and PCO_2 gradients [(A-a) DO_2 and (a-A) DCO_2] (12–14). Compared with conventional gas ventilation with 100% O_2 , there was a 50% increase in ventilation-perfusion (\dot{V}_A/\dot{Q}) heterogeneity and a 50% increase in O_2 shunt, both of which can contribute to the alveolar-arterial difference. We hypothesized, but were unable to verify experimentally, that a

diffusion barrier exists across the PFC in the lung periphery and that it is responsible for a significant portion of measured increases in alveolar-arterial differences in healthy animals during PLV. To test the feasibility of this hypothesis, we developed two mathematical models of gaseous diffusion in partially PFC-filled lung subunits.

In our experimental studies we used the multiple inert gas elimination technique (MIGET) to measure \dot{V}_A/\dot{Q} heterogeneity in healthy piglets during PLV (13, 14, 20). The use of this method raised the question of whether inert and respiratory gas exchange reaches steady state during PLV within a time frame similar to conventional gas ventilation. Steady state refers to the condition in which, given a constant source of a gas infused into mixed venous blood, the ratio of input to output partial pressures across the lung (i.e., $P_a/P_{\bar{v}}$ and $P_e/P_{\bar{v}}$, where P_a , $P_{\bar{v}}$, and P_e are arterial, mixed venous, and expired pressures, respectively) does not change with time and there is no further storage or net loss of mass within the lung over time. Using a very simple model, we showed previously that the time to steady state for SF_6 (a gas used in MIGET to estimate shunt) was prohibitively long because of its high solubility in PFC vs. blood (13). This required us to modify MIGET by eliminating SF_6 from the analysis, inasmuch as it did not satisfy the underlying assumption that steady-state conditions exist (13). With the more sophisticated models described here, we were able to refine and verify these original predictions and further explore the effects of PFC on attainment of steady-state gas exchange for the remaining five inert gases as well as O_2 and CO_2 . We are also able to explore the effect of PFC dose on diffusion-limited gas transport in the alveolus.

In recent publications, PLV has been shown to improve gas exchange in humans with acute lung injury (4, 8, 11). We have focused our efforts on studying the effects of PLV in healthy animals to shed light on the fundamental differences in gas exchange between gas- and liquid-filled lungs. Many of the equations in traditional gas exchange theory are based on the assumptions that steady-state mass flux exists and that there is a negligible diffusion barrier in the alveolus (e.g., Berggren shunt and Bohr dead space). These assumptions need to be critically evaluated in the novel situation of a fluid-filled lung. Despite mild increases in (A-a) DO_2 and (a-A) DCO_2 during PLV in healthy animals, oxygenation and ventilation can be achieved surprisingly well through a liquid-filled lung. The success of PLV in a clinical setting may depend on altering our thinking about shunt and dead space when we add a high-solubility fluid with diffusion resistance to the air

The costs of publication of this article were defrayed in part by the payment of page charges. The article must therefore be hereby marked "advertisement" in accordance with 18 U.S.C. Section 1734 solely to indicate this fact.

space of the lung. The models described here have been helpful in exploring these ideas.

MATHEMATICAL MODELS

In prior publications we presented two different models of gas exchange during PLV: 1) a two-compartment well-mixed model used to estimate times to steady state (13) and 2) a spherical gas exchange model used to estimate steady state arterial-alveolar differences across a PFC diffusion barrier (14). Here we expand on both models, adding a gas compartment to the one-dimensional well-mixed model, providing time- and space-dependent numerical solutions to the spherical model, and providing a full discussion of the underlying assumptions and model behavior. We explore solutions to the time rate of change of partial pressures of O_2 , CO_2 , and six MIGET gases in PFC after a step change in input partial pressures.

A comparison of two separate model configurations is particularly enlightening, since the *in vivo* PFC-filled alveolus probably includes some features of both. The well-stirred compartment model reflects a PFC layer with complete convective mixing and no diffusion limitation within the gas exchange unit, whereas the spherical shell model imitates a perfectly still diffusion barrier interposed between gas and blood. The true nature of gas exchange in PFC lies somewhere between these models. With each breath, PFC probably moves in and out of some alveoli and small airways and exists as small stagnant puddles in others.

Glossary

β	Solubility of a tracer gas in a solvent (ml gas · 100 ml solvent ⁻¹ · Torr ⁻¹)
C	Concentration of a tracer gas in a solvent (ml gas/ml solvent)
D	Molecular diffusion coefficient (cm ² /s)
M	Mass of tracer gas in a solvent (ml gas)
MIGET	Multiple inert gas elimination technique
n	Number of gas exchange units in a piglet lung
P	Partial pressure of a tracer gas (Torr)
PFC	Perfluorochemical
PLV	Partial liquid ventilation
\dot{Q}	Blood flow (ml/s)
RR	Respiratory rate (min ⁻¹)
r	Radial distance from center of gas compartment (cm)
r_c	Radius of gas exchange unit at the capillary boundary (cm)
r_g	Radius of gas compartment (cm)
t	Time (s)
τ	Time constant (s)
T	Temperature (°C or K)
T_{98}	Time to 98% of steady state (s)
V_D	Dead space (ml/breath)
V_T	Tidal volume (ml/breath)
a	Arterial
A	Alveolar
b	Blood
c	Capillary
g	Alveolar gas
gi	Inspired gas
pfc	Perfluorocarbon
\bar{v}	Mixed venous

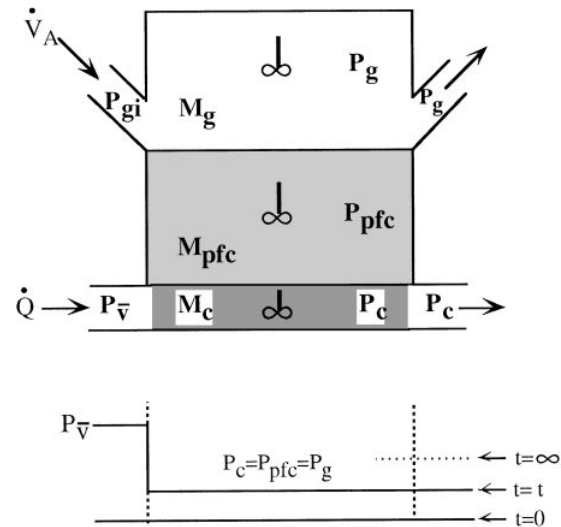


Fig. 1. Schematic of 3-compartment model with well-mixed blood, PFC, and alveolar gas compartments. Capillary compartment is perfused at a rate \dot{Q} at partial pressure $P_{\bar{v}}$. Capillary, PFC, and gas compartment partial pressures vary with time but are uniformly mixed and in spatial equilibrium at each *time t*. Partial pressure vs. distance along capillary is illustrated for a point in time. See *Glossary* for definition of abbreviations.

Model assumptions. In both models we assumed that the blood and gas compartments on either side of the PFC are well mixed. The models also assume that diffusion barriers at the capillary membrane and the PFC-gas interface are negligible. Because the presence of the PFC in the alveolar space does not affect gas exchange properties of the alveolar-capillary membrane, the assumption of complete equilibrium across the membrane is as valid as in the gas-filled lung. Blood flow and ventilation are assumed continuous and non-pulsatile (i.e., \dot{Q} and \dot{V}_A are constant).

$P_{\bar{v}}$ of tracer gases was assumed to be constant, and variation in body tissue partial pressures was assumed to be negligible. In the experimental situation, $P_{\bar{v}}$ of the inert gases will vary slightly with time as the body comes to a new steady state after a perturbation in gas exchange. We believed that this variation was small, inasmuch as the body tissues were previously equilibrated with inert gas and the recirculated component is a small fraction of the total $P_{\bar{v}}$. The error introduced by this assumption will lead to a slight underestimation of the true time to reach steady state.

Time-dependent gas exchange in a well-stirred three-compartment model. Figure 1 schematically describes this model, in which blood is delivered to the capillary compartment at a flow rate \dot{Q} (ml/s) and ventilation through the gas compartment occurs at a rate \dot{V}_A (ml/s). A tracer gas may enter the gas exchange unit dissolved in blood at partial pressure $P_{\bar{v}}$ or via ventilation at partial pressure P_{gi} . Mass balance for the tracer in three compartments is given by Eq. 1 with the assumption that the PFC layer is well mixed. Thus the gas partial pressures in all compartments are equal (i.e., $P_c = P_{pfc} = P_g$) at *time t*

$$\frac{d(M_c + M_{pfc} + M_g)}{dt} = \dot{Q} \cdot (C_{\bar{v}} - C_c) - \dot{V}_A \cdot (C_g - C_{gi}) \quad (1)$$

Converting mass ($M = C \cdot V$) and concentration ($C = \beta \cdot P$) to partial pressures (P), applying the assumption $P_c = P_{pfc} = P_g$ (i.e., well-mixed with no diffusion gradients), and rearranging into the standard form for a first-order differential equation $\tau \cdot \dot{P} + P = K$ (where τ is the time constant and K is the steady-state asymptotic value of P)

$$\frac{V_c \cdot \beta_b + V_{pfc} \cdot \beta_{pfc} + V_g \cdot \beta_g}{\dot{V}_A \cdot \beta_g + \dot{Q} \cdot \beta_b} \cdot \frac{dP_{pfc}}{dt} + P_{pfc} = \frac{\dot{V}_A \cdot \beta_g \cdot P_{gi} + \dot{Q} \cdot \beta_b \cdot P_{\bar{v}}}{\dot{V}_A \cdot \beta_g + \dot{Q} \cdot \beta_b} \tag{2}$$

τ can be expressed as follows

$$\tau = \frac{V_c + V_{pfc} \cdot \frac{\beta_{pfc}}{\beta_b} + V_g \cdot \frac{\beta_g}{\beta_b}}{\dot{V}_A \cdot \frac{\beta_g}{\beta_b} + \dot{Q}} \tag{3a}$$

The standard solution to Eq. 2 takes the form

$$P = K \cdot (1 - e^{-t/\tau}) \tag{3b}$$

where $K = [\dot{V}_A \cdot P_{gi} \cdot (\beta_g/\beta_b) + \dot{Q} \cdot P_{\bar{v}}] / [\dot{V}_A \cdot (\beta_g/\beta_b) + \dot{Q}]$.

The rate at which P_{pfc} approaches steady-state equilibrium is determined by τ , the time for the exponential term to decrease by 63%. At 4τ , steady-state equilibrium is >98% complete. The standard MIGET theory assumes that $P_c = P_g = \text{constant}$; i.e., after a change in the infusate, the time at which gas exchange measurements are taken is much longer than τ , so the exponential term in Eq. 3 becomes negligible.

Equation 3 shows that when PFC is present in the alveolus and $\beta_{pfc} > \beta_b$, τ is prolonged, especially if β_{pfc} is greater than both β_b and β_g . For gases in which this holds true, larger volumes of PFC result in longer times to equilibrium. For O_2 , τ is actually prolonged in the absence of PFC, because $\beta_g > \beta_{pfc}$. It is also prolonged as \dot{V}_A approaches zero (i.e., shunt), because PFC must equilibrate to a higher final value, i.e., input partial pressures $P_{\bar{v}}$ or P_{gi} . When \dot{V}_A is nonzero, the steady-

state partial pressure (K) is less than input partial pressure and τ is accordingly shorter. Increasing \dot{V}_A or \dot{Q} shortens τ for all gases.

Time-dependent gas exchange in a spherical shell with radial diffusion. To simulate gas exchange in a functional subunit of lung (Fig. 2), we chose a spherically shaped structure with an outer layer of capillary blood surrounding a layer of PFC that, in turn, surrounds a gas-filled center. The branching, space-filling nature of lung architecture is too complex for small-scale mathematical modeling. We chose to model gas exchange at the level of the terminal alveolar duct and represented them as smooth spheres. If the anatomic subunit is larger than this, the surface area of a smooth sphere would greatly underestimate the surface-to-volume ratio. On the other hand, representing a structure as small as an alveolus by a closed sphere would overestimate the ratio, since alveoli are roughly hexagonal cups. We therefore compromised on a structure the size of a single terminal alveolar sac to be portrayed by a sphere with dimensions derived accordingly.

We assumed that the capillary and alveolar gas compartments were individually well mixed and that uniform radial diffusion occurred in the PFC. Mass exchange between the compartments is dependent on the interfacial area bounding two adjacent regions. The area of the capillary-PFC interface is fixed at $4\pi r_c^2$. The area of the inner gas space ($4\pi r_g^2$) depends on the volume of PFC administered and on total lung volume. PFC is assumed to distribute uniformly as a spherical shell with the ventilated gas "hole" in the center. As the hole radius approaches zero, the unit becomes "flooded" with PFC. As r_g approaches r_c the model represents a gas-filled lung with no diffusion gradient (see PARAMETER ESTIMATES for description of actual dimensions used).

We use three coupled differential equations to describe mass flux between blood, PFC, and gas. Equation 4 represents the rate of change of mass ($\beta \cdot V \cdot P$) of a dissolved gas in the capillary blood compartment. It is equal to the rate of gas delivery to the capillary space via blood flow, the rate of gas removal via blood flowing out of the capillary, and the rate of diffusive gas flux

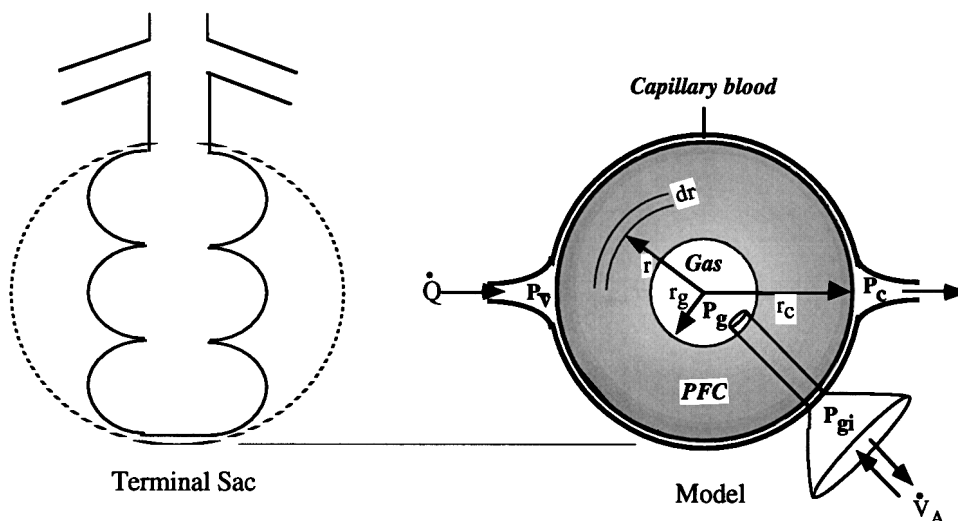


Fig. 2. Schematic of spherical shell model representing a terminal sac partially filled with PFC. Size of unit approximates a terminal alveolar sac. Gases enter model via mixed venous blood at pressure $P_{\bar{v}}$ in capillary compartment or through inspired gas at pressure P_{gi} . Gas diffuses radially (r) through PFC and is removed from system by ventilation at pressure P_g or by blood flow at pressure P_c . PFC-gas and capillary-PFC interfaces are located at $r = r_g$ and $r = r_c$, respectively. Only radial gradients in gas concentration occur. Differential volume element for analysis is a spherical shell of thickness dr . See Glossary for definition of abbreviations.

across the alveolar capillary membrane into the PFC. Equation 5 describes radial diffusion in the PFC shell, which has spherical symmetry (1). Equation 6 represents the rate of change of mass in the central air space determined by addition of gas via inspiration, subtraction of gas removed by expiration, and subtraction of gas diffusing across the air-liquid interface from the PFC layer adjacent to the compartment

$$\beta_b \cdot V_c \cdot \frac{dP_c}{dt} = \dot{Q} \cdot \beta_b \cdot (P_{\bar{v}} - P_c) - (D_{pfc} \cdot \beta_{pfc} \cdot 4 \cdot \pi \cdot r_c^2) \cdot \left. \frac{\partial P_{pfc}}{\partial r} \right|_{r=r_c} \quad (4)$$

$$\beta_{pfc} \cdot V_{pfc} \cdot \frac{\partial P_{pfc}(r, t)}{\partial t} = D_{pfc} \cdot \beta_{pfc} \cdot V_{pfc} \cdot \left(\frac{\partial^2 P_{pfc}}{\partial r^2} + \frac{2}{r} \cdot \frac{\partial P_{pfc}}{\partial r} \right) \quad (5)$$

$$\beta_g \cdot V_g \cdot \frac{dP_g}{dt} = \dot{V}_A \cdot \beta_g \cdot (P_{gi} - P_g) + (D_{pfc} \cdot \beta_{pfc} \cdot 4 \cdot \pi \cdot r_g^2) \cdot \left. \frac{\partial P_{pfc}}{\partial r} \right|_{r=r_g} \quad (6)$$

The system of three partial differential equations was solved numerically to determine the partial pressure profiles in the PFC layer from the capillary-PFC interface to the PFC-gas interface. Spatial derivatives were determined by finite difference, and time derivatives were solved using LSODE, a time-integrating algorithm developed by Hindmarsh (7). The executable program was submitted as a batch job in which each simulation was solved numerically using an IBM model RS6000 computer running Unix version 4.2. P_c and P_g are equal to $P_{pfc}(r)$ at the r_c and r_g boundaries. The time to steady-state equilibrium (T_{98}) was defined as the time for the numerical solutions to converge to 98% of the analytically determined P_c and P_g for a steady-state gas diffusion in a spherical shell, as defined by Crank (1) (see Eqs. 7-11). The two calculated mass flow rates across the capillary-PFC and PFC-gas boundaries were nearly equal at "steady state" by use of these criteria.

Steady-state gas exchange in a spherical shell with radial diffusion. Under steady-state conditions, the time rate of change of compartmental partial pressures is zero and mass flow is equal across all boundaries. We used Crank's (1) steady-state solution to Eq. 5 describing the concentration profile as a function of radial position $[C(r)]$ in a spherical shell to simplify the above system of equations and to analytically calculate blood-gas partial pressure differences

$$C(r) = \frac{r_g \cdot \beta_{pfc} \cdot P_g \cdot (r_c - r) + r_c \cdot \beta_{pfc} \cdot P_c \cdot (r - r_g)}{r \cdot (r_c - r_g)} = \beta_{pfc} \cdot P_{pfc}(r) \quad (7)$$

Differentiating Eq. 7 with respect to r , evaluating $\beta_{pfc} \cdot dP_{pfc}/dr$ at $r = r_c$ and also at $r = r_g$, and then substituting into Eqs. 4 and 6 gives

$$\dot{Q} \cdot \beta_b \cdot P_{\bar{v}} = \left(\dot{Q} \cdot \beta_b + D_{pfc} \cdot \beta_{pfc} \cdot 4\pi \frac{r_c \cdot r_g}{r_c - r_g} \right) \cdot P_c - \left(D_{pfc} \cdot \beta_{pfc} \cdot 4\pi \frac{r_c \cdot r_g}{r_c - r_g} \right) \cdot P_g \quad (8)$$

$$P_{gi} \cdot \beta_g \cdot \dot{V}_A = - \left(D_{pfc} \cdot \beta_{pfc} \cdot 4\pi \frac{r_c \cdot r_g}{r_c - r_g} \right) \cdot P_c + \left(\dot{V}_A \cdot \beta_g + D_{pfc} \cdot \beta_{pfc} \cdot 4\pi \frac{r_c \cdot r_g}{r_c - r_g} \right) \cdot P_g \quad (9)$$

Equations 8 and 9 constitute simultaneous equations in two unknowns (P_c and P_g). Substituting $K_1 = D_{pfc} \cdot 4\pi \cdot (r_c \cdot r_g)/(r_c - r_g) \cdot \beta_{pfc}/\beta_g$ and solving for P_c and P_g

$$P_c = \frac{P_{\bar{v}} \left(1 + \frac{\dot{V}_A}{K_1} + \frac{\dot{V}_A \cdot \beta_g \cdot P_{gi}}{\dot{Q} \cdot \beta_b \cdot P_{\bar{v}}} \right)}{1 + \dot{V}_A \left(\frac{1}{K_1} + \frac{\beta_g}{\dot{Q} \cdot \beta_b} \right)} \quad (10)$$

$$P_g = \frac{P_{\bar{v}} \left(1 + \frac{\dot{V}_A}{K_1} \cdot \frac{P_{gi}}{P_{\bar{v}}} + \frac{\dot{V}_A \cdot \beta_g \cdot P_{gi}}{\dot{Q} \cdot \beta_b \cdot P_{\bar{v}}} \right)}{1 + \dot{V}_A \left(\frac{1}{K_1} + \frac{\beta_g}{\dot{Q} \cdot \beta_b} \right)} \quad (11)$$

and

$$P_c - P_g = \frac{P_{\bar{v}} - P_{gi}}{1 + \frac{K_1}{\dot{V}_A} + \frac{K_1 \cdot \beta_g}{\dot{Q} \cdot \beta_b}} \quad (12)$$

At the extremes of no PFC ($r_c = r_g$) and $P_{gi} = 0$, Eqs. 10 and 11 reduce to the MIGET equations for retention (R) and excretion (E): $R = E = \lambda_b/(\lambda_b + \dot{V}_A/Q)$, where $\lambda_b = \beta_b/\beta_g$. Notice that the capillary-to-gas partial pressure ($P_c - P_g$) difference is dependent on the absolute values of \dot{V}_A and \dot{Q} .

PARAMETER ESTIMATES

Parameter values were chosen to correspond to the dimensions of lung structure and function of healthy piglets weighing 2-4 kg. Piglets this size typically have a functional residual capacity of 30 ml/kg and respiratory rate (RR) of 20 breaths/min. For calculation purposes, an average weight of 2.5 kg was used. As discussed above, our gas exchange unit represents a terminal sac in the lung of a piglet. Haefeli-Bleuer and Weibel (5) measured the outer diameter of human terminal sacs (an alveolar duct plus 2 alveoli in total width) to be $656 \pm 127 \mu\text{m}$. Tenney and Remmers (18) showed that species variation in alveolar diameter was correlated to metabolic rate per unit body weight, with adult pig alveolar diameter ~91% of the diameter of

human alveoli ($656 \times 0.91 = 597 \mu\text{m}$). On the basis of these data we chose an end-inspiratory r_c of $300 \mu\text{m}$. Surface area and volume of a single spherical unit are therefore 0.0113 cm^2 and 0.000113 cm^3 , respectively. The number (n) of terminal sacs or gas exchange units in a piglet lung was then determined by the ratio of end-inspiratory lung volume [$(48 \text{ ml/kg}) \times (2.5 \text{ kg}) = 120 \text{ ml}$ at $r_c = 300 \mu\text{m}$] to gas exchange unit volume ($1.13 \times 10^{-5} \text{ ml}$): 1,062,000 units/lung, which we rounded to 1×10^6 . End-inspiratory lung volume was determined as the sum of functional residual capacity lung volume (30 ml/kg), tidal volume (V_T , 15 ml/kg), and 3 ml/kg associated with positive end-expiratory pressure of $5 \text{ cmH}_2\text{O}$ used in all our experimental work (12). If there are 20 alveoli per terminal gas exchange unit, there would be $\sim 20 \times 10^6$ alveoli/piglet. Lung volume is obviously not constant throughout the respiratory cycle. We evaluated the steady-state model (Eqs. 10 and 11) for several lung volumes in the range of tidal breathing, i.e., r_c of 270 and $300 \mu\text{m}$, to illustrate the impact of lung volume on (A-a)DO₂ and (a-A)DCO₂. We did not simulate tidal breathing in the sense of second-to-second variation in V_g .

Ventilation per gas exchange unit (V_A) was determined using our typical experimental V_T of 15 ml/kg (12), estimated dead space (V_D) of 4.5 ml/kg , RR of 20 min^{-1} , M of 2.5 kg , and n as follows: $V_A = (V_T - V_D) \cdot \text{RR} \cdot M/n = 8.74 \times 10^{-6} \text{ ml/s}$. Blood flow per gas exchange unit (Q) was derived from average piglet cardiac output of 500 ml/min (12) divided by n : $8.33 \times 10^{-6} \text{ ml/s}$. The capillary blood volume was derived on the basis of anatomic data that show pulmonary capillaries to cover 75% of the alveolar surface (i.e., capillary surface area per spherical model unit = $0.75 \times 0.0113 \text{ cm}^2$) and have a thickness equivalent to the red cell diameter ($5 \mu\text{m}$), giving a V_c per unit of $4.24 \times 10^{-6} \text{ ml}$. The volume of PFC per gas exchange unit (V_{pfc}) was determined from the total dose of PFC divided by n . For example, a dose of 30 ml/kg in a 2.5-kg piglet results in a total dose of 75 ml , or V_{pfc} of $7.5 \times 10^{-5} \text{ ml/unit}$. PFC layer thickness is dependent on r_c and the volume of PFC present, with the assumption that PFC is distributed as a spherical shell with a gas hole in the center (Fig. 2). Normal parameter values for the spherical model under matched V_A/Q and V_{pfc} of 30 ml/kg are summarized in Table 1.

Values of β_b and β_{pfc} for inert gases were obtained from experimental measurements of gas solubility in pig blood and in the PFC perflubron ($\text{C}_8\text{F}_{17}\text{Br}$, Liqui-

Table 1. Normal model parameters for $\dot{V}_A/\dot{Q} = 1$ and $V_{\text{pfc}} = 30 \text{ ml/kg}$

Parameter	Description	Value
r_g	Gas volume radius	$210 \mu\text{m}$
r_c	Gas exchange unit radius	$300 \mu\text{m}$
V_c	Capillary volume	$4.24 \times 10^{-6} \text{ ml}$
D_{pfc}	Diffusion coeff in PFC	$4.36 \times 10^{-5} \text{ cm}^2/\text{s}$
V_A	Exchange unit ventilation	$8.74 \times 10^{-6} \text{ ml/s}$
Q	Exchange unit blood flow	$8.33 \times 10^{-6} \text{ ml/s}$
n	No. of exchange units	1×10^6

PFC, perfluorocarbon.

Table 2. Solubilities of 6 inert gases, O_2 , and CO_2 in blood and PFC

Gas	β_b	β_{pfc}
SF_6	0.000974 ± 0.000049	0.410 ± 0.065
Ethane	0.0116 ± 0.0047	0.234 ± 0.026
Cyclopropane	0.0749 ± 0.0078	0.791 ± 0.052
Halothane	0.396 ± 0.047	0.826 ± 0.066
Ether	1.34 ± 0.036	5.08 ± 0.19
Acetone	38.4 ± 0.42	3.86 ± 0.37
O_2	0.003	0.0658
CO_2	0.779	0.256

Values are expressed in $\text{ml gas} \cdot 100 \text{ ml solvent}^{-1} \cdot 100 \text{ Torr}^{-1}$. Inert gas solubilities in pig blood (β_b , $n = 9$, means \pm SE) and in PFC (β_{pfc} , $n = 6$, means \pm SE) were measured by gas chromatography with flame ionization detector and electron capture. O_2 and CO_2 solubilities in blood are described in PARAMETER ESTIMATES. "Solubility" in gas (β_g) is 0.132 for all gases.

Vent, Alliance Pharmaceutical, San Diego, CA) (12). The "solubility" of a tracer gas in the gas phase (β_g) is defined in the classic paper by Piiper et al. (16) as $0.00132 \text{ Torr}^{-1}$ ($=1/760$ at sea level).

The solubility of O_2 and CO_2 in blood was determined by the slope of the curve of gas content vs. partial pressure. This relationship is nonlinear over the physiological range of partial pressures of these gases because of chemical binding in the blood. O_2 combines with Hb, resulting in an S-shaped concentration vs. pressure curve in the partial pressure range $0\text{--}150 \text{ Torr}$. For $\text{PO}_2 > 150 \text{ Torr}$, the concentration vs. partial pressure curve is linear, because Hb is saturated, and for O_2 , β_b is the same as in plasma: $0.003 \text{ ml} \cdot 100 \text{ ml solvent}^{-1} \cdot \text{Torr}^{-1}$. For $\text{PO}_2 < 150 \text{ Torr}$, β_b for O_2 is much higher; e.g., at PO_2 of 40 Torr it is $0.06 \text{ ml} \cdot 100 \text{ ml solvent}^{-1} \cdot \text{Torr}^{-1}$ as determined by the slope of the O_2 content (CO_2 , $\text{ml O}_2/100 \text{ ml blood}$) vs. PO_2 (Torr) curve generated by the subroutines of Olszowka and Farhi (15). For the steady-state partial pressure differences calculated using Eqs. 10 and 11, we used only β_b for O_2 of 0.003 , because for all the experimental data against which we are comparing model results arterial PO_2 (Pa_{O_2}) was $> 150 \text{ Torr}$ (12). The solubility of CO_2 in blood is a function of dissolved CO_2 as well as CO_2 converted to HCO_3^- . The content (C_{CO_2}) vs. PCO_2 curve is approximately linear within $40\text{--}80 \text{ Torr PCO}_2$. With use of the blood-gas routines of Olszowka and Farhi, β_b for CO_2 was determined from the slope of C_{CO_2} vs. PCO_2 over this range and was found to be $0.779 \text{ ml} \cdot 100 \text{ ml blood}^{-1} \cdot \text{Torr}^{-1}$. O_2 and CO_2 solubilities in PFC were provided by Alliance Pharmaceutical (Table 2).

Few molecular diffusion coefficients (D_{pfc}) of dissolved gases in PFC are precisely known. Tham et al. (19) measured D_{pfc} of O_2 and CO_2 in three perfluorochemicals (Caroxin-D, Caroxin-F, and FC-80), finding the average diffusion coefficient for O_2 in PFC to be $5.61 \times 10^{-5} \text{ cm}^2/\text{s}$ at 37°C with a range of $5.57\text{--}5.65 \times 10^{-5} \text{ cm}^2/\text{s}$ and for CO_2 in PFC at 37°C to be $4.36 \times 10^{-5} \text{ cm}^2/\text{s}$ with a range of $4.21\text{--}4.48 \times 10^{-5} \text{ cm}^2/\text{s}$. The diffusion coefficients of O_2 and CO_2 in H_2O at 37°C are 3.3×10^{-5} and $2.6 \times 10^{-5} \text{ cm}^2/\text{s}$, respectively (6).

We used the average value of the CO_2 diffusion coefficient as measured by Tham et al. (19) to estimate

D_{pfc} of each respiratory gas in perflubron, the PFC used in our experiments. There are no experimental data available measuring diffusivity in PFC of the six inert gases used in MIGET (9, 20). Their diffusivities in H_2O at 37°C are $1.63 \times 10^{-5} \text{ cm}^2/\text{s}$ for SF_6 , $1.96 \times 10^{-5} \text{ cm}^2/\text{s}$ for ethane, $1.84 \times 10^{-5} \text{ cm}^2/\text{s}$ for cyclopropane, $1.28 \times 10^{-5} \text{ cm}^2/\text{s}$ for halothane, $0.85 \times 10^{-5} \text{ cm}^2/\text{s}$ for ether, and $1.62 \times 10^{-5} \text{ cm}^2/\text{s}$ for acetone (17, 21). Because their diffusivities in H_2O are only slightly less than those of CO_2 in H_2O , we chose the value of D_{pfc} for CO_2 in PFC to represent the diffusivity of the six inert gases in the absence of experimental data.

RESULTS

Solutions for both of the models were well behaved with no instances of negative results or mass imbalance. Partial pressures at the boundaries between compartments were continuous. The numerically integrated time- and space-dependent solutions for the spherical model converged on the analytic steady-state solutions. For each of the eight gases simulated, the time to steady-state equilibrium was estimated by two independent models, and the times generated by both models were within 30% of each other and usually within 10%.

Time to reach steady-state equilibrium. Figure 3 illustrates the time rate of change of partial pressure of the eight gases in the simpler well-mixed three-compartment model with V_{pfc} of 30 ml/kg after a step change in the input partial pressure of each gas. For O_2 this involved setting P_{gi} at 650 Torr and P_{v} at 40 Torr and for the remaining 7 gases P_{gi} at 0 Torr and P_{v} at 1 Torr at *time 0*. Figure 3A illustrates the application of Eq. 3 for normal conditions of matched \dot{V}_A and \dot{Q} ($\dot{V}_A/\dot{Q} = 1$). Figure 3B illustrates the same for near-zero ventilation (shunt conditions). Because O_2 is delivered by ventilation, PO_2 was not simulated for shunt conditions. Whenever \dot{V}_A is negligible, Eq. 3 shows that the final value is always P_{v} , and the time constants are lengthened. Both features are apparent in Fig. 3B. Gases with the lowest $\beta_b/\beta_{\text{pfc}}$ ratio (i.e., SF_6) take the longest to equilibrate, because PFC acts as a large capacitor that fills slowly when there is great disparity in solubilities.

Figure 4 demonstrates the time and space rate of change in the spherical gas exchange unit with 30 ml/kg PFC and matched \dot{V}_A and \dot{Q} (as described in PARAMETER ESTIMATES). Figure 4A shows successive time traces of PCO_2 vs. radial distance from the capillary through PFC to the central gas region. After a step change in P_{v} from 0 to 40 Torr, PCO_2 increases in the gas exchange unit until it converges on the steady-state value. Figure 4B shows similar successive time traces of PO_2 vs. radial distance through the PFC after a step change in P_{gi} from 0 to 650 Torr.

Table 3 reports the T_{98} for eight gases in each of the two models with V_{pfc} of 30 ml/kg. T_{98} values were defined slightly differently for the two models. In the well-mixed model T_{98} was defined as 4τ in Eq. 3; for the spherical model it was the time at which the time-dependent solutions (Eqs. 4–6) converged to 98% of the

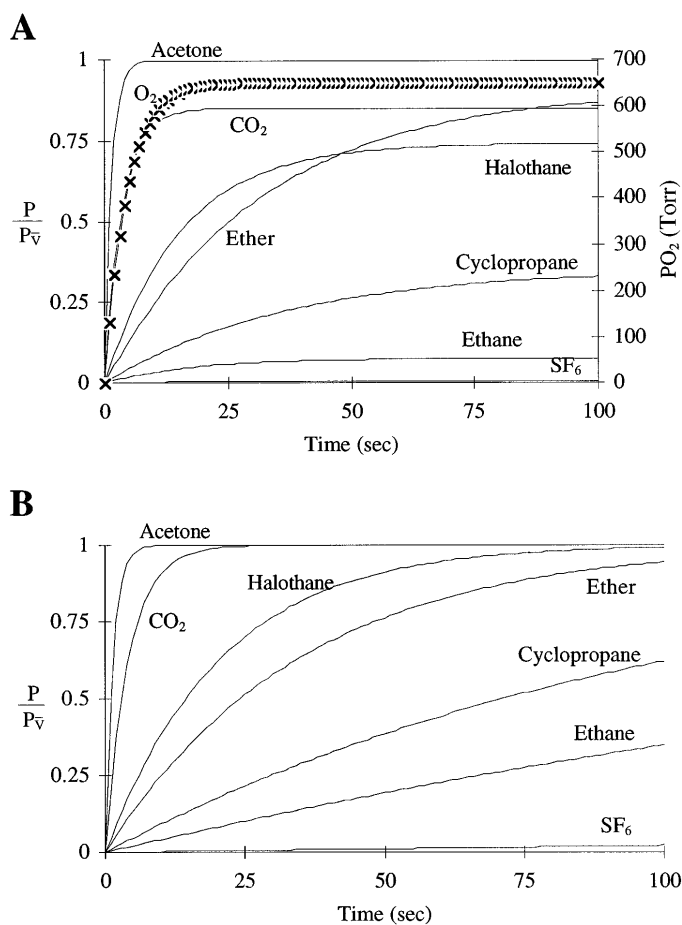


Fig. 3. Normalized partial pressure (P/P_{v}) vs. time of 6 inert gases, O_2 , and CO_2 in well-mixed 3-compartment model with $V_{\text{pfc}} = 30$ ml/kg. P represents $P_c = P_{\text{pfc}} = P_g$ in well-mixed model, β values are as described in PARAMETER ESTIMATES. $P_{\text{gi}} = 0$ and $P_{\text{v}} = 1$ for 6 inert gases and CO_2 (smooth lines); for O_2 $P_{\text{gi}} = 650$ and $P_{\text{v}} = 0$. A: solutions for normal conditions ($\dot{V}_A = 8.74 \times 10^{-6}$ ml/s and $\dot{Q} = 8.33 \times 10^{-6}$ ml/s) after a step change in P_{v} or P_{gi} at *time 0*. B: solutions for shuntlike conditions ($\dot{V}_A = 0$ and $\dot{Q} = 8.33 \times 10^{-6}$ ml/s) after a step change in input partial pressures. T_{98} values are given in Table 3.

analytic steady-state solutions (Eqs. 10 and 11). We evaluated the model for three conditions to illustrate the range of T_{98} likely to be encountered in the lung partially filled with PFC: matched \dot{V}_A and \dot{Q} , \dot{V}_A approximately zero with \dot{Q} normal (shunt), and \dot{Q} near zero with \dot{V}_A normal (dead space).

For \dot{V}_A and \dot{Q} well-matched ($\dot{V}_A/\dot{Q} = 1$), all times to steady state were <3 min. The gas with the longest time to steady state was cyclopropane followed by ether, SF_6 , halothane, O_2 , CO_2 , and acetone. Under shunt conditions all times to steady state were prolonged (except for acetone, which is insensitive to shunt), with SF_6 having the longest times at ~ 5 h. The time to steady state for O_2 was also markedly prolonged at ~ 27 min, whereas that for CO_2 remained short at 15–20 s. Under dead space conditions the times were intermediate, with the longest being for acetone at ~ 26 min. CO_2 equilibration times were mildly prolonged under these conditions, ~ 95 s.

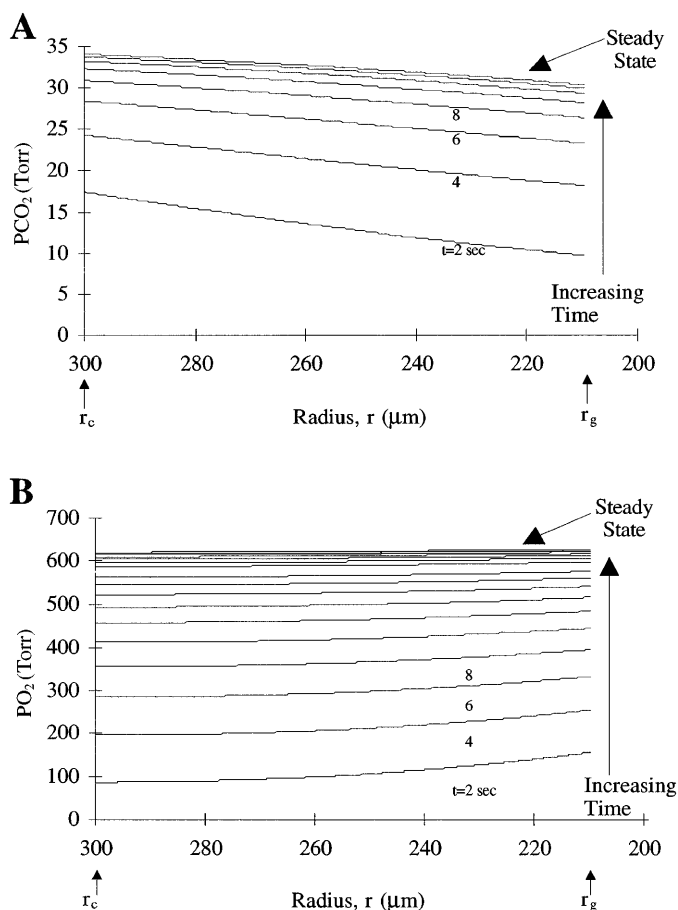


Fig. 4. Examples of time- and space-dependent changes in PCO_2 (A) and PO_2 (B) in spherical shell model. Multiple tracings represent P in PFC layer vs. r at 2-s intervals after a step change in $P_{\bar{v}}$ of 40 Torr PCO_2 (A) or in P_{gi} of 650 Torr PO_2 with $P_{\bar{v}} = 40$ (B). Solutions converge on steady-state values. $P_c = P_{\text{pfc}}$ at $r = r_c$ and $P_g = P_{\text{pfc}}$ at $r = r_g$. Model parameters for these solutions are as follows: $V_{\text{pfc}} = 30$ ml/kg, $r_c = 300$ μm , $r_g = 210$ μm , $\dot{V}_A = 8.74 \times 10^{-6}$ ml/s, and $\dot{Q} = 8.33 \times 10^{-6}$ ml/s. V_c , D , and β values are defined in PARAMETER ESTIMATES.

Steady-state gas exchange in a PFC-filled spherical shell. Steady-state partial pressure differences of inert and respiratory gases were calculated from Eqs. 10 and 11. SF_6 was left out of the following discussion, since it was not included in our experimental MIGET analysis (12, 13) because of its prohibitively long time to reach steady state under shunt conditions. Figure 5 shows P_c - P_g differences of seven gases normalized by input partial pressure ($P_{\bar{v}}$ for the 5 inert gases and CO_2 and P_{gi} for O_2) vs. r_g for \dot{V}_A of 8.74×10^{-6} ml/s and \dot{Q} of 8.33×10^{-6} ml/s. An r_g of 0 corresponds to a flooded terminal sac with no gas compartment, and r_g of 300 μm corresponds to a gas exchange unit with no PFC. Values of r_g equal to 210, 250, and 280 μm correspond to the three doses of PFC used in our experimental work: 30, 20, and 10 ml/kg, respectively (12). CO_2 shows the largest difference at all values of r_g , with the P_c - P_g difference nearly 10% of the input pressure at r_g of 210 μm . The partial pressure gradient of O_2 is very low at the same dose ($<1\%$ of P_{gi}), rising only when r_g becomes very small as the gas exchange unit becomes flooded with PFC. The inert gases also show a negligible P_c - P_g

Table 3. T_{98} after a step change in input partial pressure ($P_{\bar{v}}$ or P_{gi}) with $V_{\text{pfc}} = 30$ ml/kg and $r_c = 300$ μm

Gas	T_{98} , s					
	Normal ($\dot{V}_A = 8.74 \times 10^{-6}$, $\dot{Q} = 8.33 \times 10^{-6}$)		Quasi-shunt ($\dot{V}_A = 8.74 \times 10^{-9} \approx 0$, $\dot{Q} = 8.33 \times 10^{-9}$)		Quasi-dead space ($\dot{V}_A = 8.74 \times 10^{-6}$, $\dot{Q} = 8.33 \times 10^{-9} \approx 0$)	
	Well mixed	Radial diffusion	Well mixed	Radial diffusion	Well mixed	Radial diffusion
SF_6	122.87	123.69	17,538.07	15,025.79	123.73	107.4
Ethane	72.33	73.81	933.10	906.03	78.40	84.49
Cyclopropane	144.76	143	411.57	404.66	223.29	221.93
Halothane	61.28	61.59	82.65	83.48	237.08	235.16
Ether	126.14	125.21	139.13	138.44	1,350.45	1,311.19
Acetone	5.67	7.64	5.69	7.64	1,581.69	1,214.99
O_2	34.06	36.14	1,601.64	1,505.63	34.80	47.85
CO_2	14.36	16.29	16.91	20.36	95.41	97.22

T_{98} , time to reach 98% steady-state partial pressure. Solutions for well-mixed 3-compartment model are compared with those for spherical model with radial diffusion for 3 combinations of varying ventilation (\dot{V}_A) and perfusion (\dot{Q}).

difference for r_g of 210 μm , with halothane having the largest P_c - P_g difference at 3% of $P_{\bar{v}}$ followed by cyclopropane, ethane, acetone, and ether. As the PFC layer increases in thickness, the P_c - P_g difference rises exponentially, approaching $P_{\bar{v}}$ values for CO_2 and the inert gases and P_{gi} for O_2 . For these simulations, $P_{\bar{v}}$ for O_2 was set to zero and P_{gi} to 1 for the sake of comparison.

Figure 6 illustrates the effect of gas exchange unit volume ("lung volume") on partial pressure difference of O_2 and CO_2 . Although our model does not incorporate features of tidal breathing, we explored the effect of varying the gas exchange unit volume between the extremes of end inspiration ($r_c = 300$ μm) and end

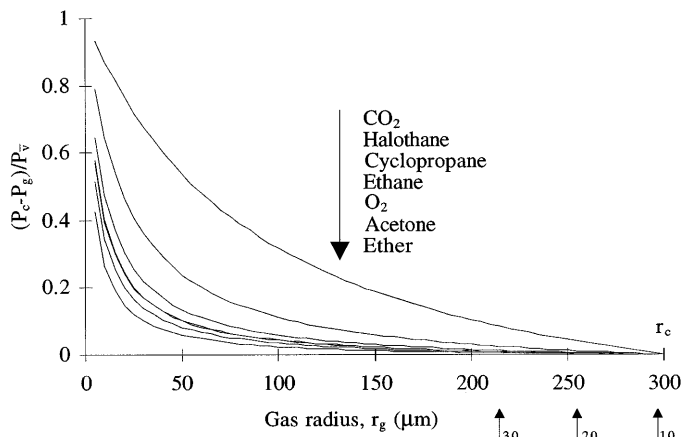


Fig. 5. Spherical shell model. Steady-state normalized and capillary-to-gas partial pressure (P_c - P_g) differences are shown vs. PFC thickness for 5 inert gases plus O_2 and CO_2 . Radial thickness of PFC is varied from 0 (no PFC present, $r_g = r_c$) to 300 μm (all PFC, $r_g = 0$). Arrows under abscissa indicate r_g corresponding to 30, 20, and 10 ml/kg doses of PFC. V_c , D , and β are defined in PARAMETER ESTIMATES; V_{pfc} and V_g vary with r_g ; $P_{\text{gi}} = 0$ and $P_{\bar{v}} = 1$ for all inert gases. $\dot{V}_A = 8.74 \times 10^{-6}$ ml/s and $\dot{Q} = 8.33 \times 10^{-6}$ ml/s. Top curve is for CO_2 , bottom curve is for ether, and other curves are for gases in sequence shown. O_2 and ethane are indistinguishable. Capillary-to-gas disequilibrium is, by far, the largest for CO_2 .

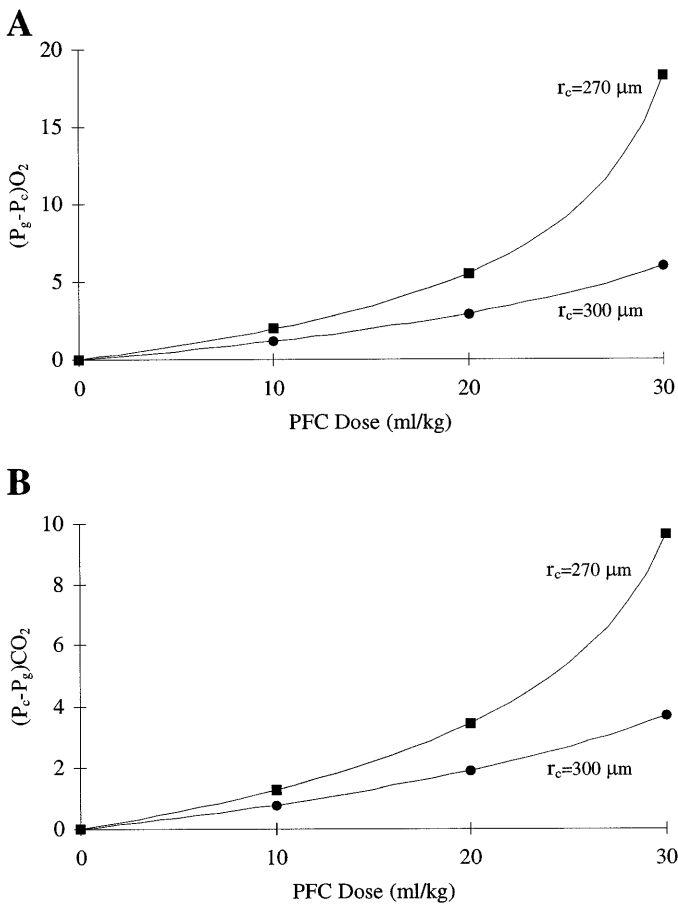


Fig. 6. $P_c - P_g$ difference for O_2 and CO_2 vs. PFC dose at a high gas-exchange unit volume (\bullet) and a low gas-exchange unit volume (\blacksquare) for $\dot{V}_A = 8.74 \times 10^{-6}$ ml/s and $\dot{Q} = 8.33 \times 10^{-6}$ ml/s. D and β values are defined in PARAMETER ESTIMATES. A: $P_g - P_c$ difference for O_2 for $P_{\bar{v}} = 40$ Torr and $P_{gi} = 650$ Torr rises with dose and with smaller volumes. B: $P_c - P_g$ difference for CO_2 with $P_{\bar{v}} = 40$ Torr and $P_{gi} = 0$ Torr shows the same trend as in A.

expiration ($r_c = 270 \mu m$). This might be equivalent to breath-holding maneuvers at the extremes of cyclic breathing. For both gases, the $P_c - P_g$ difference increased at the lower lung volume for all PFC doses. The percent increase in the $P_c - P_g$ difference was greater with larger doses of PFC. The $P_c - P_g$ difference for CO_2 with a $P_{\bar{v}}$ of 40 Torr and 30 ml/kg PFC in the lung varied from 3.7 Torr at the large lung volume to 9.6 Torr at the lower lung volume. At the small PFC dose of 10 ml/kg, the $P_c - P_g$ difference for CO_2 varied from 0.8 to 1.2 with the change in lung volume. We previously showed (a-A) DCO_2 in healthy animals with 30 ml/kg PFC in the lungs to be 12 Torr (12). The difference for $P_c - P_g$ difference for O_2 varied in a similar manner with an increase from 6 to 18 Torr as the gas exchange unit volume decreased with 30 ml/kg PFC in the lung and P_{gi} of 650 Torr.

We examined the impact of varying \dot{V}_A and \dot{Q} independently on the $P_c - P_g$ difference for inert gases, O_2 , and CO_2 . At PFC thicknesses up to 100 μm (PFC dose ~ 30 ml/kg), varying \dot{V}_A and \dot{Q} had a small impact on MIGET gas $P_c - P_g$ differences. At PFC thicknesses $> 100 \mu m$, the gradients increased exponentially, as in the case of

matched \dot{V}_A and \dot{Q} (Fig. 5). The $P_c - P_g$ difference for the inert gases never exceeded 10% of $P_{\bar{v}}$ over this range of \dot{V}_A and \dot{Q} . Each gas was affected to a different degree depending on their relative solubilities. Figure 7 illustrates the effect of varying \dot{V}_A and \dot{Q} on O_2 and CO_2 . Figure 7A shows minimal effect on the $P_g - P_c$ difference for O_2 with varying \dot{V}_A over a range from 0.1 to 10 times the average ventilation of a terminal alveolar sac (8.74×10^{-6} ml/s) with \dot{Q} fixed (8.33×10^{-6} ml/s). Figure 7B shows an 8-fold increase in the $P_g - P_c$ difference for O_2 with a 10-fold increase in \dot{Q} . The gradient drops to near zero as \dot{Q} decreases to 0.1 its average value. Changes in partial pressure differences of CO_2 with varying \dot{V}_A and \dot{Q} are shown in Fig. 7, C and D. There is a 3-fold increase in the $P_c - P_g$ difference with \dot{V}_A 10 times its average value, and the gradient drops to near zero with \dot{V}_A at 0.1 its average value. The $P_c - P_g$ difference for CO_2 drops in half with a decrease in \dot{Q} but is essentially unchanged with a 10-fold increase in \dot{Q} . Comparison of the solutions $10 \times \dot{V}_A$ and $0.1 \times \dot{Q}$ in Fig. 7, A and B, as well as 7, C and D, illustrates that the $P_c - P_g$ gradient is different for each condition, despite equivalent \dot{V}_A/\dot{Q} ratios.

DISCUSSION

Evaluation of model assumptions. We had two specific questions in mind when developing these models of gas exchange in a terminal sac filled with PFC: 1) Do gases that are exchanged in a PFC-containing alveolus reach steady state at usual respiratory rates? 2) How large are the alveolar-arterial differences as a result of diffusion across PFC barriers? Two different models were developed in an attempt to answer these questions. The well-mixed three-compartment model provided a simple approach to estimating time to steady state. Its major assumptions are that neither diffusion times in the PFC nor the geometry of a gas-exchanging subunit significantly affect the solutions. By contrast, our spherical model explicitly incorporated the diffusion gradients and more realistic geometry but, despite major mathematical differences, the results showed very close agreement with the well-mixed compartment model predictions of time to steady state (Table 3).

Both models depict gas exchange in a single terminal alveolar sac. Parameters such as \dot{Q} , \dot{V}_A , and V_{pfc} were arrived at by partitioning an equal amount of \dot{Q} , \dot{V}_T , and V_{pfc} to all terminal sacs in the lung. The lung is not homogeneous in its distribution of any of these parameters, and application of model results to interpretation of experimental data must be done with this in mind. In reality, there will be a heterogeneous distribution of gas exchange units ranging from completely PFC filled to partially PFC filled to completely gas filled that are ventilated and perfused in some heterogeneous distribution. Measured arterial and expired gas partial pressures are weighted averages of gas exchange subunits. Model predictions of gas exchange in a single terminal sac help us explore the range of possible alveolar $P_c - P_g$ differences due to diffusion limitation and provide a gross approximation to overall lung arterial-alveolar differences.

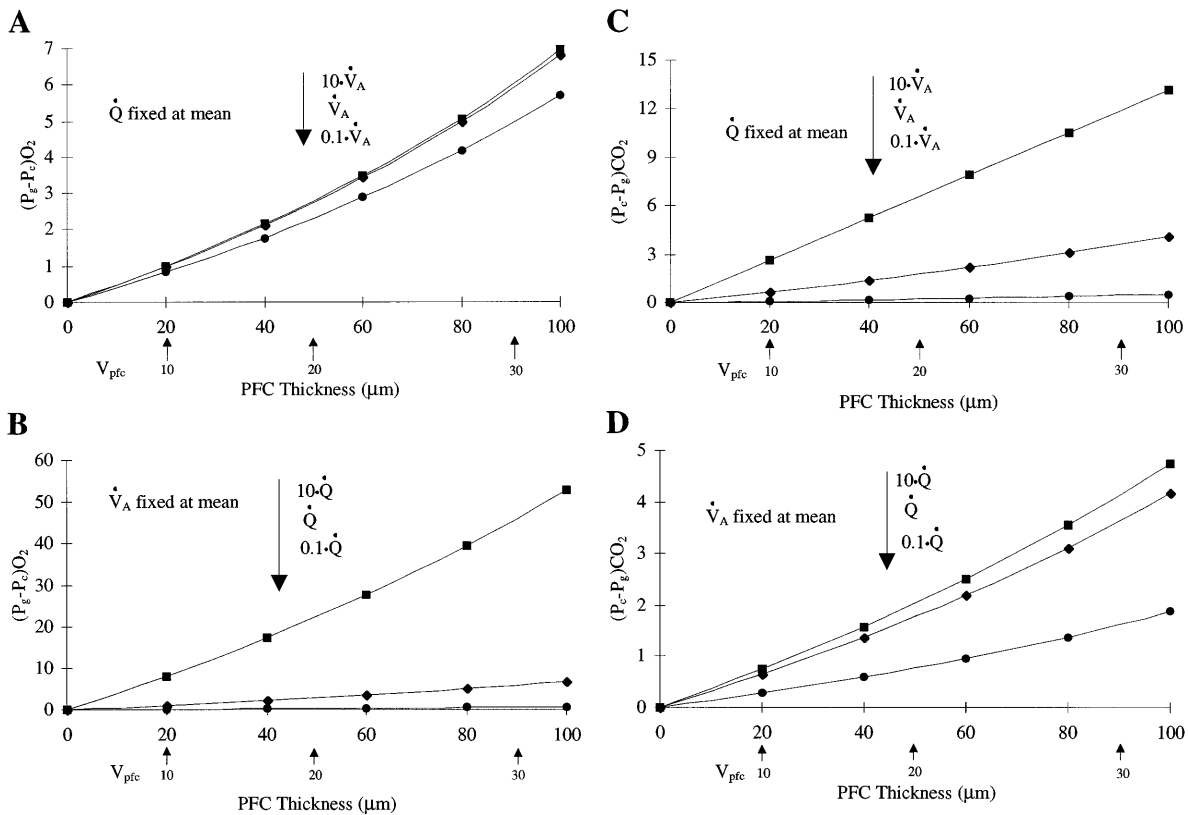


Fig. 7. $P_g - P_c$ difference for O_2 (A and B) and $P_c - P_g$ differences for CO_2 (C and D) vs. PFC thickness, with \dot{V}_A or \dot{Q} varied while the other is fixed at a mean value ($\dot{V}_A = 8.74 \times 10^{-6}$ ml/s and $\dot{Q} = 8.33 \times 10^{-6}$ ml/s). Radial thickness of PFC ranges from 0 (no PFC present) to 100 μm ; arrows under abscissa indicate r_g corresponding to $V_{pfc} = 10, 20,$ and 30 ml/kg with $r_c = 300 \mu\text{m}$. $V_c, D,$ and β values are defined in PARAMETER ESTIMATES. For $CO_2, P_v = 40$ Torr and $P_{gi} = 0$ Torr; for $O_2, P_v = 40$ Torr and $P_{gi} = 650$ Torr. A: $P_g - P_c$ difference for O_2 is relatively insensitive to variation in \dot{V}_A from 0.1 to 10 times its average value. B: $P_g - P_c$ for O_2 rises 8-fold with a 10-fold increase in \dot{Q} and drops to near zero at 0.1 its average value. C and D: sensitivity of $P_c - P_g$ difference for CO_2 to variations in \dot{V}_A and \dot{Q} from 0.1 to 10 times their average value.

Additionally, the choice of a spherical shape of our gas exchange unit to approximate the terminal alveolar sac likely overestimates the diffusion barrier somewhat. A terminal sac is not a smooth sphere but, rather, a cluster of cup-shaped alveoli opening up to a common duct. There are sheets of perfused alveolar-capillary membrane extending inward toward the duct that increase the surface area for exchange and bring those parts of the membrane close to the PFC-gas interface. This would be equivalent to “thinning” the PFC spherical shell in our model and decreasing the $P_c - P_g$ gradient for ventilated units. On the other hand, regions of shunt where \dot{V}_A is zero probably behave similarly to the model as the PFC pool equilibrates with mixed venous blood and geometry becomes irrelevant.

We feel justified in our choice of inert gas diffusion coefficients on the basis of the fact that the inert gases and CO_2 had similar diffusion coefficients in H_2O and that all should have increased diffusivity in perflubron because it is a nonpolar solvent. The rate of diffusion of a molecule through a fluid medium depends on the “effective radius” of the molecule, a function of molecular size and van der Waals interactions with neighboring molecules. Increased D_{pfc} for O_2 and CO_2 in PFC compared with H_2O suggests that the molecules have

smaller effective volumes in PFC because of reduced van der Waals interactions. Although there are certain to be discrepancies between the true diffusion coefficients of these gases in PFC and our approximated D_{pfc} , model results show little dependence of our time- or space-dependent solutions on diffusive resistance. As we demonstrate, the disparity in $P_c - P_g$ gradients for different gases with the same D_{pfc} (i.e., CO_2 vs. ether) supports the conclusion that minor variations in D_{pfc} will not significantly affect our model results.

Time to reach steady state. Of particular interest to us was whether the inert gases used in MIGET would reach steady state during PLV within the time period of our experimental measurements (12, 13). In using MIGET to assess \dot{V}_A/\dot{Q} heterogeneity in healthy piglets during PLV, we modified the standard protocol (9, 20) to incorporate a 60-min equilibration period between experimental conditions (15 min is more common). Results from our two models suggest that all gases come to equilibrium well within this time period with the exception of SF_6 under shunt conditions (>4 h). We showed this previously and eliminated SF_6 from MIGET analyses during PLV (12, 13). The remaining five inert gases reach steady state within the 1-h time frame. The next longest equilibration time was for acetone, which

took ~26 min to come to steady state under “dead space” conditions ($\dot{Q} = 0$). Except for one case, O_2 and CO_2 reached steady state in <2 min for the range of possible \dot{V}_A and \dot{Q} that might exist during PLV. O_2 took 26.6 min to reach steady state under shunt conditions because of the slow delivery rate.

We did not incorporate the periodic nature of \dot{V}_A and \dot{Q} in our model, but this would be a useful extension. It would be interesting to see if O_2 and CO_2 reach steady state, despite breath-to-breath variations in P_g and pulsatile changes in P_c that occur over a 2- to 4-s time period. Intuition leads us to think that a gas exchange unit would reach steady state about an average value of P_c and P_g , filtering out second-to-second fluctuations.

Partial pressure differences at steady state. PFC acts as a mild diffusion barrier for all gases in the steady state, creating a P_c - P_g difference that increases with volume of liquid in the alveolar space (Fig. 5). Less intuitive is the fact that the partial pressure gradient for each gas is different on the basis of the relative solubility of the gas in blood, PFC, and the gas phase. The presence of a partial pressure gradient in alveoli during steady-state gas exchange has several important consequences. Gas exchange efficiency is reduced with overall arterial-alveolar partial pressure gradients increased compared with healthy gas-filled lung. This impacts gas exchange calculations using formulas derived for the gas-filled lung such as the Berggren shunt, Bohr dead space, and the model underlying MIGET. Each will be in error by an amount proportional to the partial pressure gradient in the alveolus.

The alveolar gas exchange model underlying MIGET (9, 20) assumes no diffusion gradient in the alveolus

$$P_c/P_{\bar{v}} = P_g/P_{\bar{v}} = \lambda_b/(\lambda_b + \dot{V}_A/\dot{Q})$$

This equation compares with our *Eqs. 10 and 11*, which reduce to this simpler case when P_{gi} is zero and r_g equals r_c (no fluid in the alveolus). There is a variable effect of PFC on the P_c - P_g difference of each of the five inert gases, with halothane and cyclopropane showing the largest gradients (Fig. 5). However, we have shown through model solution for a wide range of PFC thickness, \dot{V}_A , and \dot{Q} that P_c - P_g is very small compared with the driving pressure, $P_{\bar{v}}$, for the inert gases, except when alveoli are flooded with PFC. This would lead us to conclude that the more complicated model in this paper is insignificantly different from that underlying the MIGET model, except in the case of flooded alveoli. In this extreme case, MIGET should detect shunt as P_c and P_g diverge in the same way retention and excretion curves separate at low \dot{V}_A/\dot{Q} (9, 20). In addition, the smoothing algorithm employed by MIGET to fit an S-shaped curve to measured data points will smooth out the nonsystematic differences in retention and excretion that result from interaction with the PFC.

Further inspection of *Eqs. 10 and 11* shows that when PFC is present, differences between P_c and P_g are a function of solubility in each of the three media: D , \dot{V}_A/\dot{Q} , and \dot{V}_A independent of \dot{Q} . This last point is a significant departure from the theoretical framework of

MIGET as well as our understanding of \dot{V}_A/\dot{Q} heterogeneity as it affects gas exchange physiology. Our model shows that P_c and P_g are dependent on the absolute values of \dot{V}_A and \dot{Q} during PLV. Figure 7B shows that the P_c - P_g difference for O_2 is very sensitive to \dot{Q} (at fixed \dot{V}_A), with the gradient widening when \dot{Q} is high and becoming negligible when \dot{Q} is very small. Variation of \dot{V}_A produces little change in the O_2 gradient for given \dot{Q} (Fig. 7B). Partial pressure differences for CO_2 show the opposite: increasing with high \dot{V}_A , becoming negligible with low \dot{V}_A , and changing little with \dot{Q} (Fig. 7, C and D). This is similar to gas exchange in gas-filled lungs where Pa_{O_2} is sensitive to shunt and arterial PCO_2 (Pa_{CO_2}) is sensitive to dead space. The difference is that during PLV the absolute value of \dot{V}_A and \dot{Q} independent of \dot{V}_A/\dot{Q} will affect overall gas exchange. This may be the most significant pitfall in the use of MIGET during PLV, inasmuch as it does not incorporate this feature in the basic model. The implications are that regions of higher-than-average blood flow will have greater (A-a) DO_2 and those with higher than average ventilation result in larger (a-A) D CO_2 . Pooling of PFC in dependent regions of lung that receive a greater proportion of blood flow may exacerbate this effect.

Partial pressure gradients of O_2 in the partially PFC-filled gas exchange unit with an inspiratory O_2 fraction of 650 Torr ranges from 1.2 Torr for a 10 ml/kg dose at high lung volumes to 18 Torr for a 30 ml/kg dose at low lung volumes (Fig. 6A). The P_g - P_c gradient for O_2 is maximal for an unventilated pool of PFC approaching a P_{gi} - $P_{\bar{v}}$ difference of ~600 Torr. The partial pressure differences in ventilated gas exchange units with 10, 20, and 30 ml/kg doses (Fig. 6A) are negligible compared with measured (A-a) DO_2 in piglets during PLV, which ranged from 150 to 320 Torr (14). We concluded that diffusion limitation does not significantly contribute to measured (A-a) DO_2 (or Berggren shunt) in partly PFC-filled, ventilated gas exchange units. It does contribute to the alveolar-arterial gradient in cases where the unit is nearly filled with PFC (Fig. 5, gas radius <50 μ m). In this situation, Berggren shunt would reflect true shunt (blood flow to unventilated regions of lung) as well as blood flow to PFC-flooded regions of lung. Changes in PFC dosing, ventilator strategies, and patient positioning designed to decrease the population of flooded gas exchange units may help decrease shunt during PLV.

CO_2 shows the greatest degree of disequilibrium at the level of the terminal sac due, in part, to its relative insolubility in PFC compared with blood (Table 2). CO_2 retention has not been a problem during PLV, primarily because of ease of adjustment of ventilation to optimize CO_2 elimination. In our experimental studies we found an increase in Pa_{CO_2} during PLV when holding minute ventilation constant (12–14). Figures 5, 6B, and 7, C and D, illustrate the degree of PCO_2 disequilibrium in the terminal alveolar sac over a range of PFC volumes, lung volumes, and \dot{V}_A and \dot{Q} . In an “average” gas exchange unit during PLV, the P_c - P_g gradient for CO_2 was as much as 10 Torr for a 30 ml/kg dose at low lung volumes and <1 Torr for a 10 ml/kg dose at high lung

volumes (Fig. 6B). Introduction of ventilation heterogeneity broadens the range of partial pressure differences even further with a P_c - P_g gradient for CO_2 of 13.2 Torr for a 30 ml/kg dose and \dot{V}_A 10 times larger than average (Fig. 7C). Large airway mixing and heterogeneity of PFC and ventilation distribution will likely produce global (a-A)DCO₂ somewhere between these extremes. We measured an (a-A)DCO₂ of 12 Torr during PLV with 30 ml/kg PFC in healthy piglets (14). This suggests that diffusion limitation could be responsible for a significant portion of (a-A)DCO₂ in this animal model during PLV.

Dead space ventilation (\dot{V}_D , ml/min) is classically determined using mass balance and substitution to arrive at the following equation: $\dot{V}_D/\dot{V}_T = (\text{Pa}_{\text{CO}_2} - \text{PE}_{\text{CO}_2})/\text{Pa}_{\text{CO}_2}$, where PE_{CO_2} is expired PCO_2 . The final form of this equation is arrived at by making the assumption that alveolar PCO_2 (PA_{CO_2}) equals Pa_{CO_2} , so that each of the terms on the right-hand side of the equation are measurable. This assumption leads to significant overestimation of \dot{V}_D when a diffusion gradient exists in the alveolus. For example, in a lung with true \dot{V}_D of 10% and (a-A)DCO₂ of 10 Torr (e.g., $\text{Pa}_{\text{CO}_2} = 40$ Torr and $\text{PA}_{\text{CO}_2} = 30$ Torr), substitution of Pa_{CO_2} for PA_{CO_2} results in an estimated \dot{V}_D/\dot{V}_T of 32%! One could argue that the effect of diffusion limitation on (a-A)DCO₂ is equivalent to that of \dot{V}_D , and we should call this "effective dead space" just as we could call flooded alveoli "shunt" in place of diffusion-limited O₂ exchange. The advantage of thinking about PFC as a diffusion barrier is that maneuvers can be performed to alter its effects, such as decreasing the total volume of PFC given or rotating the subject to redistribute pooled fluid. This may be preferable to increasing \dot{V}_T or RR to decrease "dead space" that predisposes to barotrauma.

Summary. Increased shunt during PLV in healthy animals (12) is due to flooded gas exchange units in which the PFC-gas interface is located in small airways throughout the respiratory cycle. Alveoli that are partly filled with PFC (the air-liquid interface resides inside the terminal sac) do not contribute significantly to measured (A-a)DO₂. In contrast, any amount of PFC in alveoli causes a significant increase in (a-A)DCO₂ by virtue of the gas's low solubility in PFC relative to blood. Thus diffusion-limited gas exchange during PLV is an important mechanism of impaired CO₂ elimination and less important for oxygenation.

A very interesting result of our modeling effort was the realization that gas exchange during PLV is dependent on the absolute value of \dot{V}_A and \dot{Q} , and not simply their ratio \dot{V}_A/\dot{Q} . This increases the complexity of gas exchange analysis and may be the most important reason why MIGET is not applicable in the analysis of gas exchange during PLV. Further work needs to be done to fully investigate this novel situation.

The results of this modeling effort reflect gas exchange in healthy, uncompromised lungs. In diffuse lung injury, gas exchange is improved during PLV (2, 4, 8, 10, 11) because of the combined effects of reduced surface tension and improved delivery of O₂ to edematous areas of lung. We hope that this study may be used

to help optimize the treatment of acute respiratory distress syndrome with PLV by illustrating some of the basic principles and limitations of gas exchange through a fluorocarbon medium. PLV is an exciting new methodology in the treatment of diffuse lung injury, and we hope this modeling effort stimulates further refinement of the technique.

This work was supported in part by National Heart, Lung, and Blood Institute Grant HL-12174. We are grateful to Alliance Pharmaceutical for also supporting research efforts in this field.

Present address of E. M. vanLöbenSels: Dept. of Medicine, Virginia Mason Medical Center, C8-IMA, 1100 Ninth Ave., PO Box 900, Seattle, WA 98111.

Address for reprint requests: M. P. Hlastala, Div. of Pulmonary and Critical Care Medicine, Box 356522, University of Washington, Seattle, WA 98195-6522.

Received 12 January 1998; accepted in final form 15 September 1998.

REFERENCES

1. Crank, J. *The Mathematics of Diffusion*. Oxford, UK: Clarendon, 1970.
2. Curtis, S. E., J. T. Peek, and D. R. Kelly. Partial liquid breathing with perflubron improves arterial oxygenation in acute canine lung injury. *J. Appl. Physiol.* 75: 2696-2702, 1993.
3. Fuhrman, B. P., P. R. Paczan, and M. DeFrancis. Perfluorocarbon-associated gas exchange. *Crit. Care Med.* 19: 712-722, 1991.
4. Gauger, P. G., T. Pranikoff, R. J. Schreiner, F. W. Moler, and R. B. Hirschl. Initial experience with partial liquid ventilation in pediatric patients with acute respiratory distress syndrome. *Crit. Care Med.* 24: 16-22, 1996.
5. Haefeli-Bleuer, B., and E. R. Weibel. Morphometry of the human pulmonary acinus. *Anat. Rec.* 220: 401-414, 1988.
6. Himmelblau, D. M. Diffusion of dissolved gases in liquids. *Chem. Rev.* 64: 527-550, 1964.
7. Hindmarsh, A. *LSODE*. Livermore, CA: Lawrence Livermore Laboratory, 1981.
8. Hirschl, R. B., T. Pranikoff, C. Wise, M. C. Overbeck, P. Gauger, R. J. Schreiner, R. Dechert, and R. H. Bartlett. Initial experience with partial liquid ventilation in adult patients with the acute respiratory distress syndrome. *JAMA* 275: 383-389, 1996.
9. Hlastala, M. P. Multiple inert gas elimination technique. *J. Appl. Physiol.* 56: 1-7, 1984.
10. Leach, C. L., B. P. Fuhrman, F. C. Morin, and M. G. Rath. Perfluorocarbon-associated gas exchange (partial liquid ventilation) in respiratory distress syndrome: a prospective, randomized, controlled study. *Crit. Care Med.* 21: 1270-1278, 1993.
11. Leach, C. L., J. S. Greenspan, S. D. Tubenstein, T. H. Shaffer, M. R. Wolfson, J. C. Jackson, R. Delemos, and B. P. Fuhrman. Partial liquid ventilation with perflubron in premature infants with severe respiratory distress syndrome. *N. Engl. J. Med.* 335: 761-767, 1996.
12. Mates, E. A., J. Hildebrandt, J. C. Jackson, P. Tarczy-Hornoch, and M. P. Hlastala. Shunt and ventilation-perfusion distribution during partial liquid ventilation in healthy piglets. *J. Appl. Physiol.* 82: 933-942, 1997.
13. Mates, E. A., J. C. Jackson, J. Hildebrandt, W. E. Truog, T. A. Standaert, and M. P. Hlastala. Respiratory gas exchange and inert gas retention during partial liquid ventilation. In: *Oxygen Transport to Tissue XVI*, edited by M. C. Hogan. New York: Plenum, 1994, vol. 361, p. 427-435.
14. Mates, E. A., P. Tarczy-Hornoch, J. Hildebrandt, J. C. Jackson, and M. P. Hlastala. Negative slope of exhaled CO₂ profile: implications for ventilation heterogeneity during partial liquid ventilation. In: *Oxygen Transport to Tissue XVII*, edited by C. Ince. New York: Plenum, 1996, vol. 388, p. 585-597.

15. **Olszowka, A. J., and L. E. Farhi.** A system of digital computer subroutines for blood gas calculations. *J. Appl. Physiol.* 4: 270–280, 1968.
16. **Piiper, J., P. Dejours, P. Haab, and H. Rahn.** Concepts and basic quantities in gas exchange physiology. *Respir. Physiol.* 13: 292–304, 1971.
17. **Souders, J. E., S. C. George, N. L. Polissar, E. R. Swenson, and M. P. Hlastala.** Tracheal gas exchange: perfusion-related differences in inert gas elimination. *J. Appl. Physiol.* 79: 918–928, 1995.
18. **Tenny, S. M., and J. E. Remmers.** Comparative quantitative morphology of the mammalian lung: diffusing area. *Nature* 19: 54–56, 1963.
19. **Tham, M. K., R. D. Walker, and J. H. Modell.** Diffusion coefficients of O₂, N₂ and CO₂ in fluorinated ethers. *J. Chem. Eng. Data* 18: 411–412, 1973.
20. **Wagner, P. D., H. A. Saltzman, and J. B. West.** Measurement of continuous distributions of ventilation-perfusion ratios: theory. *J. Appl. Physiol.* 36: 588–599, 1974.
21. **Wilke, C. R., and P. Chang.** Correlation of diffusion coefficients in dilute solutions. *Am. Inst. Chem. Eng. J.* 1: 264–270, 1955.

